Supplementary Materials

S1 : Mixing lines used for calculation of the end-member composition of the Fatu Kapa fluids.

S2 : Modified after Von Damm et al. (1991). Plot of the molality of dissolved SiO_2 in equilibrium with quartz in seawater versus temperature for isobars from 1500 to 1000 bars according to Von Damm et al. model. The Si most enriched fluid collected at Kulo Lasi is represented by the blue star. The red circle covers the range of Si concentrations and T encountered in fluids from the Fatu Kapa vent field.

S3 : Modified after Bischoff and Pitzer (1989). Stars stand for Kulo Lasi fluid phases characteristics. They nearly plot on the 150 bars isobar. The close up of the 400 °C – 300 bar region shows that seawater could produce the observed salinities at Kulo Lasi by phase separation at about 320-350 bars and 415-420 °C.

S4 : Modified after Kawagucci et al. (2013). Plots of H_2 concentration versus CH_4 concentration in various hydrothermal fluids. The grey area represents values observed in a hydrothermal experiment using natural seafloor sediments. Values obtained for the Wallis and Futuna vent fields are reported: Kulo Lasi brine and condensed vapour phases are marked by the red square and the blue diamond, respectively, and the blue shaded area covers the range of values obtained in the Fatu Kapa field.

S5 : Modified after Lupton et al. (2015). (a) Plot summarizing $^3He/^4He$ ratio versus $C/^3He$ for various mantle provinces, including mid-ocean ridges (black-filled symbols), submarine arc volcanoes (blue), and sub aerial arc volcanoes (green). Values for the Fatu Kapa vent field are reported as orange diamonds. $^3He/^4He$ is expressed as R/Ra. Crosses indicate average values for MORBs and for sub aerial arcs from. (b) Similar plot including values for hotspot volcanoes such as Loihi, Kilauea fumarole, Yellowstone Park gases, Reunion, and Fatu Kapa (orange diamonds).

S6 : Distribution of linear fatty acids in various environments. Data are from (Blumenberg et al., 2007) for Massive Sulphide Deposits (MSD) ; (McCollom et al., 2015) for Lost City (LC) fluids; (Cooper and Bray, 1963) for petroleum, recent and ancient sediments; (Ben-Mlih et al., 1992) for 13°N mussels.

S7 : Distribution of linear alkanes obtained by thermogenic maturation in various crude oil basins and abiotic Fischer-Tropsch Type experiment (McCollom and Seewald, 2006).

S8 : Example of a post-processed video sequence using the Typhoon algorithm to estimate displacements (instantaneous – left panel; averaged on 25 frames – right panel) on one of the small black smokers in the Kulo Lasi caldera.

S9 : Example of a post-processed video sequence using the Typhoon algorithm to estimate displacements (instantaneous – left panel; averaged on 25 frames – right panel) at the base of the Carla chimney.

S10 : Example of a post-processed video sequence using the Typhoon algorithm to estimate displacements (instantaneous – left panel; averaged on 25 frames – right panel) at the top of the massive $Obel^X$ chimney.

S11 : Time series of the estimated displacements corresponding on the video sequences shown in figures S8, S9 and S10.

References

Ben-Mlih, F., Marty, J.C., Fiala-Médioni, A., 1992. Fatty acid composition in deep hydrothermal vent symbiotic bivalves. Journal of Lipid Research 33, 1797-1806.

Bischoff, J.L., Pitzer, K.S., 1989. Liquid-vapor relations for the system NaCl-H 2 O; summary of the P-T-x surface from 300 degrees to 500 degrees C. Am J Sci 289, 217-248.

Blumenberg, M., Seifert, R., Petersen, S., Michaelis, W., 2007. Biosignatures present in a hydrothermal massive sulfide from the Mid-Atlantic Ridge. Geobiology 5, 435-450.

Cooper, J.E., Bray, E.E., 1963. A postulated role of fatty acids in petroleum formation. Geochimica et Cosmochimica Acta 27, 1113-1127.

Kawagucci, S., Ueno, Y., Takai, K., Toki, T., Ito, M., Inoue, K., Makabe, A., Yoshida, N., Muramatsu, Y., Takahata, N., Sano, Y., Narita, T., Teranishi, G., Obata, H., Nakagawa, S., Nunoura, T., Gamo, T., 2013. Geochemical origin of hydrothermal fluid methane in sediment-associated fields and its relevance to the geographical distribution of whole hydrothermal circulation. Chemical Geology 339, 213-225.

Lupton, J., Rubin, K.H., Arculus, R., Lilley, M., Butterfield, D., Resing, J., Baker, E., Embley, R., 2015. Helium isotope, C/3He, and Ba-Nb-Ti signatures in the northern Lau Basin: Distinguishing arc, back-arc, and hotspot affinities. Geochemistry, Geophysics, Geosystems 16, 1133-1155.

McCollom, T.M., Seewald, J.S., 2006. Carbon isotope composition of organic compounds produced by abiotic synthesis under hydrothermal conditions. Earth and Planetary Science Letters 243, 74-84.

McCollom, T.M., Seewald, J.S., German, C.R., 2015. Investigation of extractable organic compounds in deep-sea hydrothermal vent fluids along the Mid-Atlantic Ridge. Geochimica et Cosmochimica Acta 156, 122-144.

Von Damm, K.L., Bischoff, J.L., Rosenbauer, R.J., 1991. Quartz solubility in hydrothermal seawater; an experimental study and equation describing quartz solubility for up to 0.5 M NaCl solutions. American Journal of Science 291, 977-1007.

Figure S1

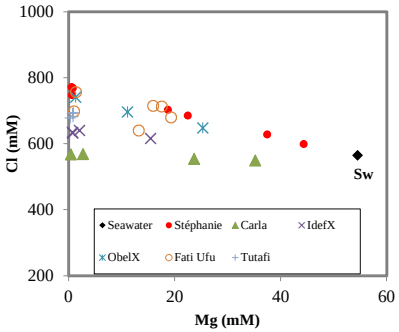
Cl (mM)
Mg (mM)
Sw
Seawater
Stéphanie
Carla
IdefX
ObelX
Fati Ufu
Tutafi

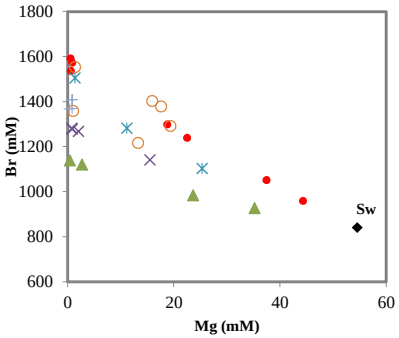
Br (mM)
Mg (mM)
Sw

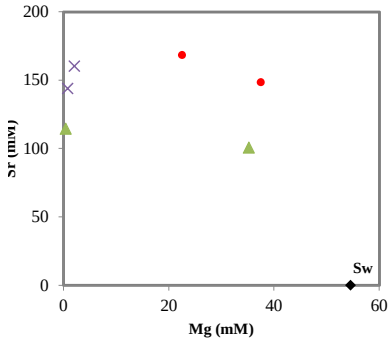
Mg (mM)
Sw

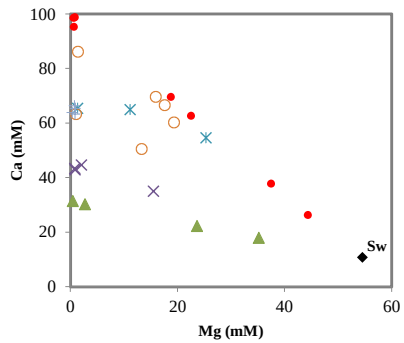
Ca (mM)
Mg (mM)
Sw

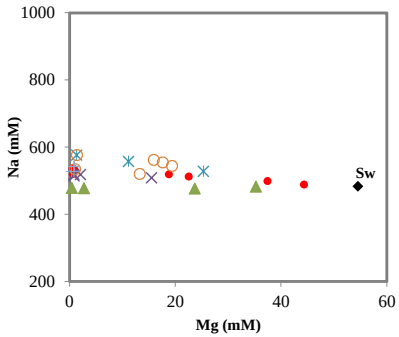
Na (mM)
Mg (mM)
Sw

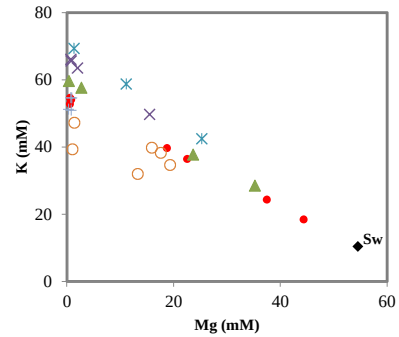
K (mM)
Mg (mM)
Sw

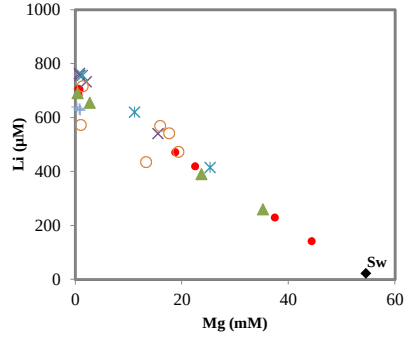
Li (µM)
Mg (mM)
Sw

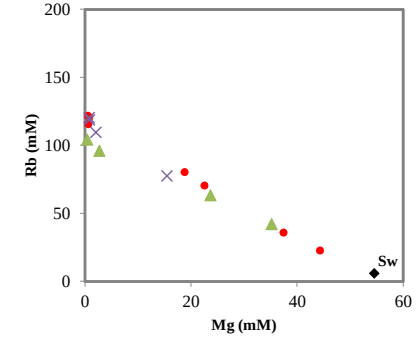
Rb (mM)
Mg (mM)
Sw

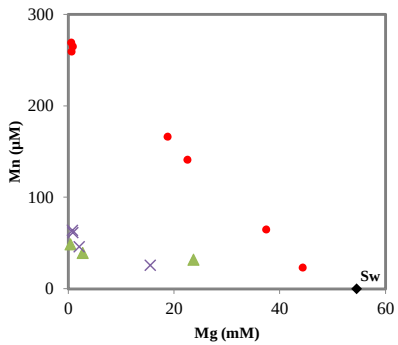
Mn (µM)
Mg (mM)
Sw

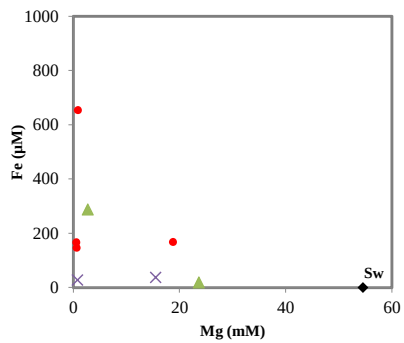
Fe (µM)
Mg (mM)
Sw

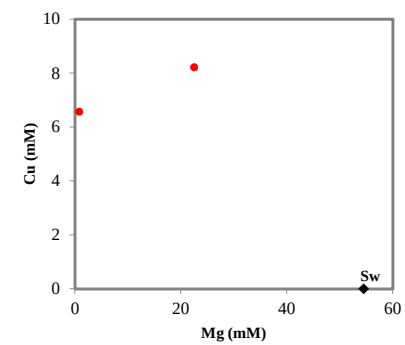
Cu (mM)
Mg (mM)
Sw

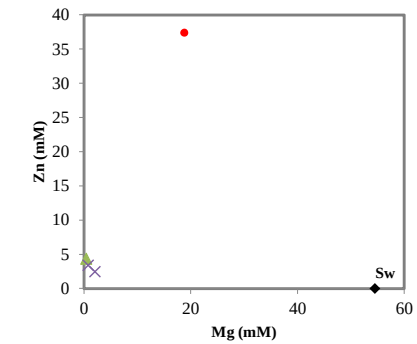
Zn (mM)
Mg (mM)
Sw

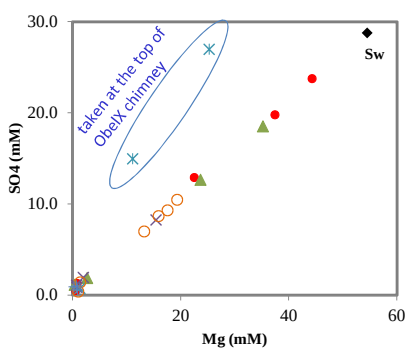
SO4 (mM)
Mg (mM)
Sw
taken at the top of ObelX chimney

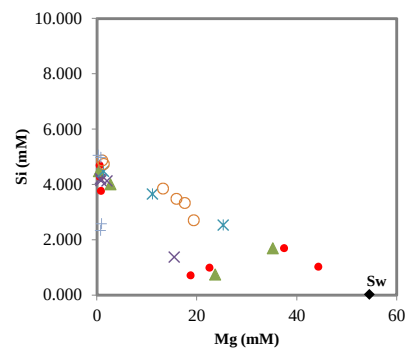
Si (mM)
Mg (mM)
Sw

Figure S2

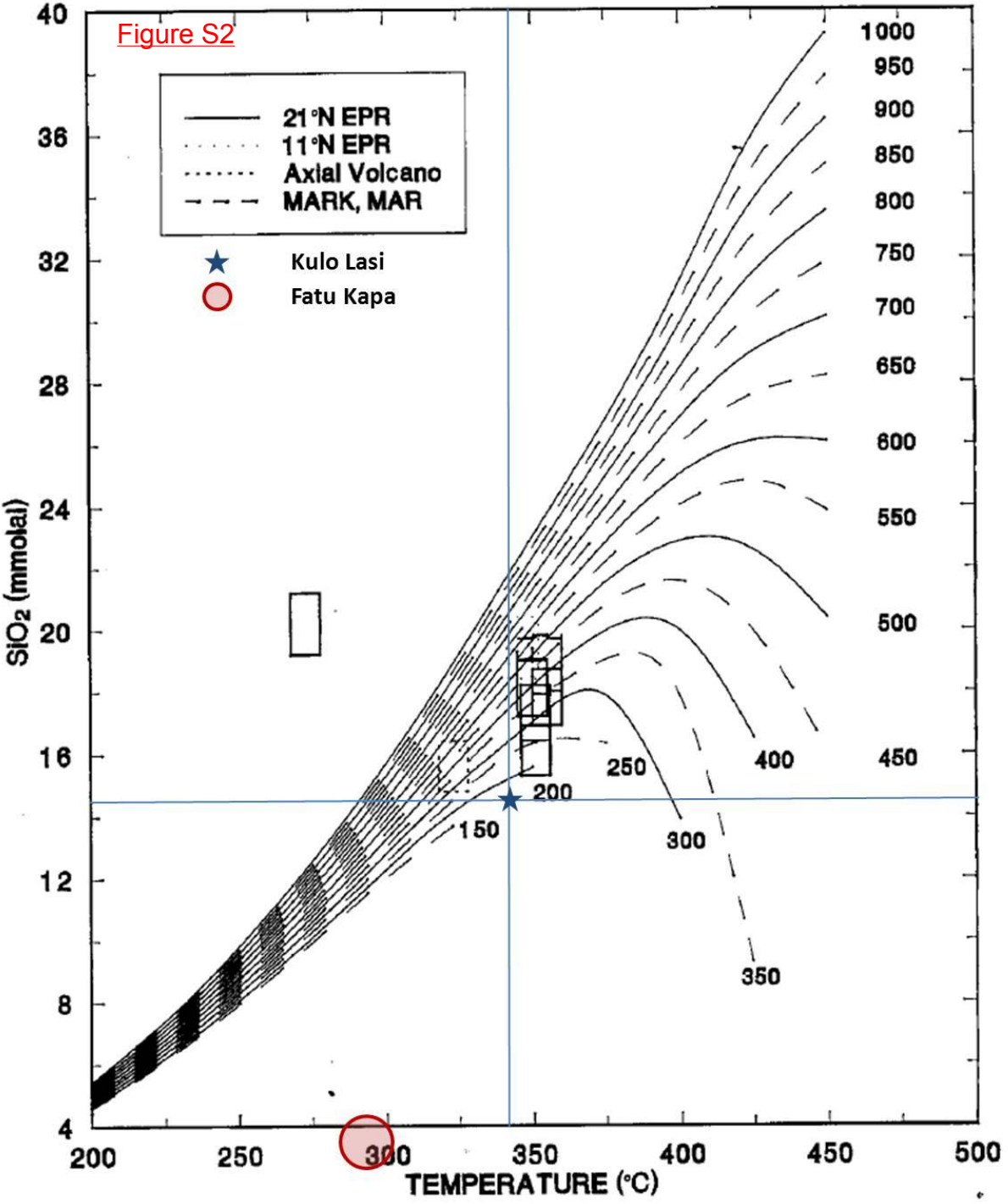
21°N EPR
11°N EPR
Axial Volcano
MARK, MAR
Kulo Lasi
Fatu Kapa
SiO2 (mmolal)
TEMPERATURE (°C)
40
36
32
28
24
20
16
12
8
4
200
250
300
350
400
450
500
1000
950
900
850
800
750
700
650
600
550
500
450
150
200
250
300
350
400

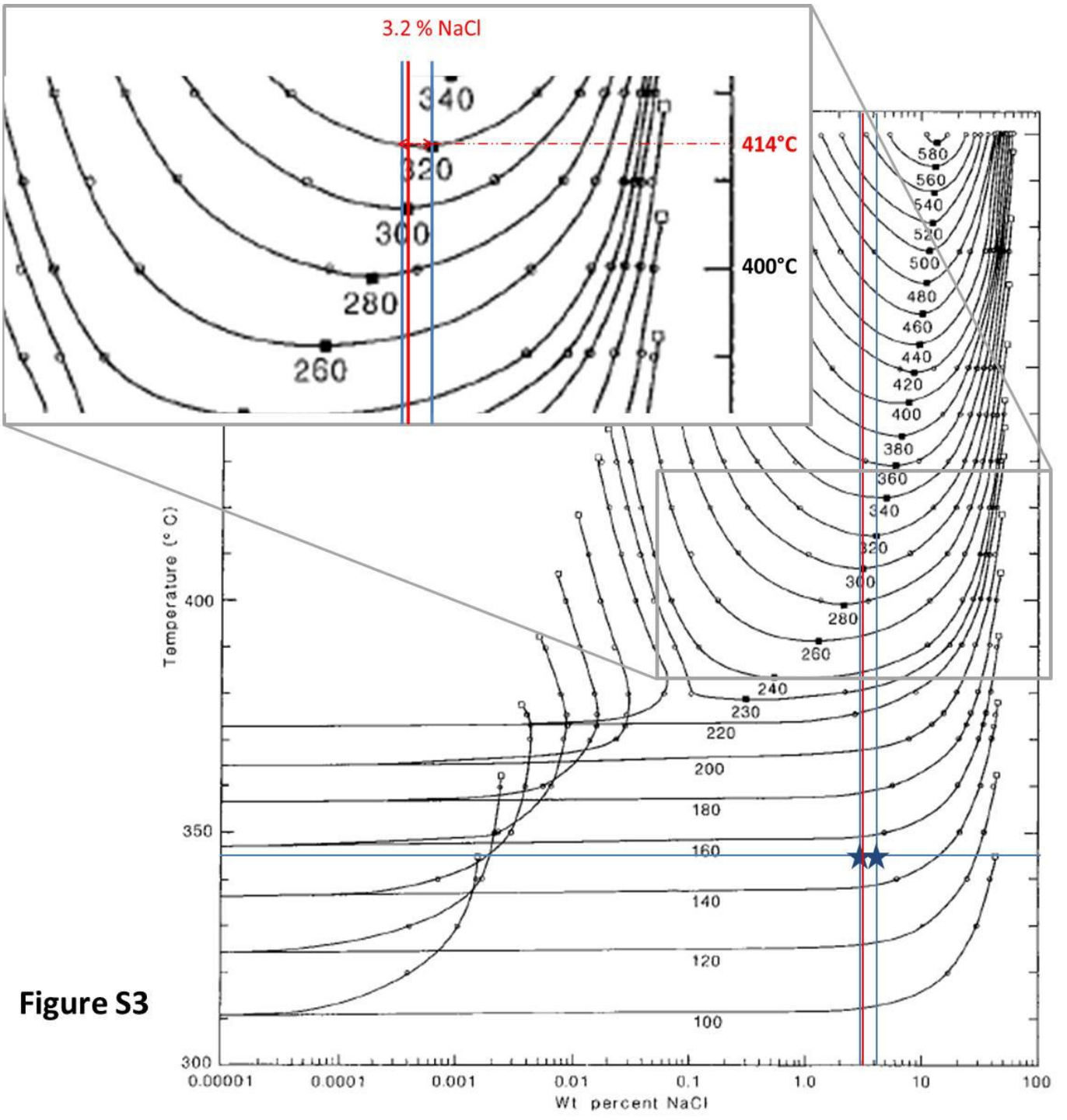
3.2 % NaCl
414°C
400°C
340
320
300
280
260
580
560
540
520
500
480
460
440
420
400
380
360
340
320
300
280
260
240
230
220
200
180
160
140
120
100
Temperature (° C)
400
350
300
0.00001
0.0001
0.001
0.01
0.1
1.0
10
100
Wt percent NaCl

Figure S3

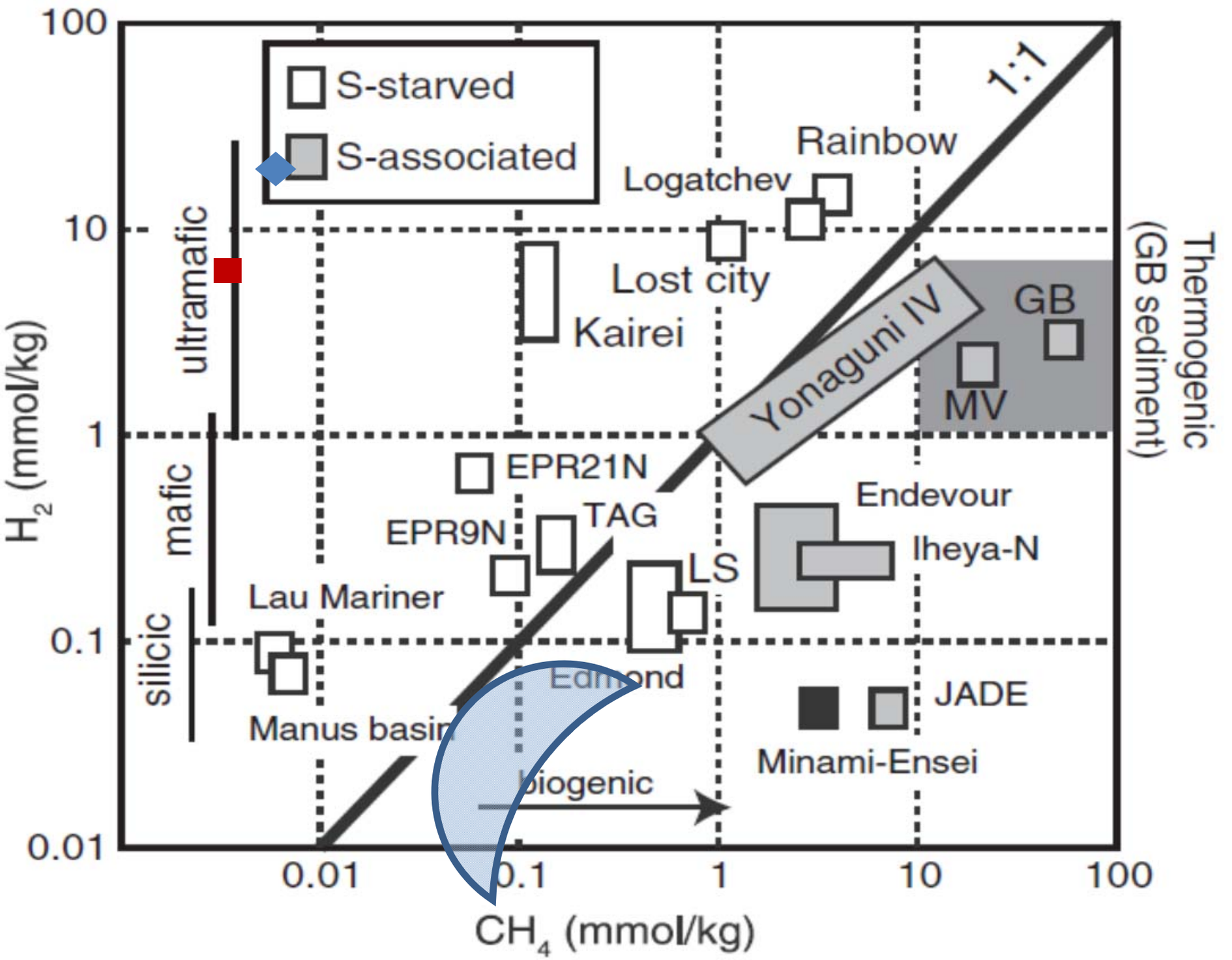
S-starved
S-associated
1:1
Rainbow
Logatchev
Lost city
Kairei
ultramafic
mafic
silicic
Yonaguni IV
GB
MV
EPR21N
EPR9N
TAG
Endevour
Iheya-N
LS
Lau Mariner
Edmond
JADE
Manus basin
Minami-Ensei
biogenic
Thermogenic
(GB sediment)
H2 (mmol/kg)
CH4 (mmol/kg)
100
10
1
0.1
0.01
0.01
0.1
1
10
100

Figure S4

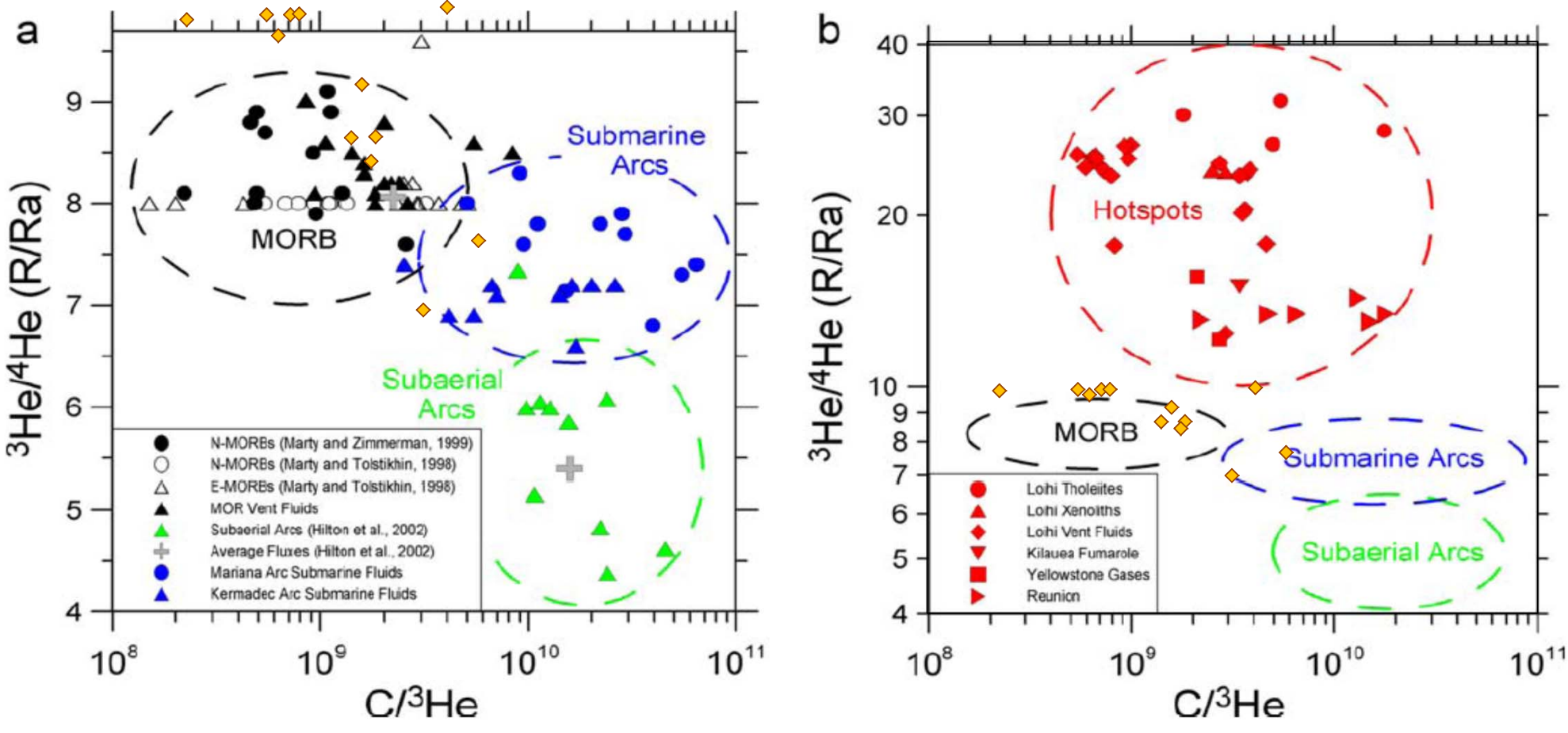
a
$^3He/^4He$ (R/Ra)
$C/^3He$
MORB
Submarine Arcs
Subaerial Arcs
N-MORBs (Marty and Zimmerman, 1999)
N-MORBs (Marty and Tolstikhin, 1998)
E-MORBs (Marty and Tolstikhin, 1998)
MOR Vent Fluids
Subaerial Arcs (Hilton et al., 2002)
Average Fluxes (Hilton et al., 2002)
Mariana Arc Submarine Fluids
Kermadec Arc Submarine Fluids
b
$^3He/^4He$ (R/Ra)
$C/^3He$
Hotspots
MORB
Submarine Arcs
Subaerial Arcs
Loihi Tholeiites
Loihi Xenoliths
Loihi Vent Fluids
Kilauea Fumarole
Yellowstone Gases
Reunion

Figure S5

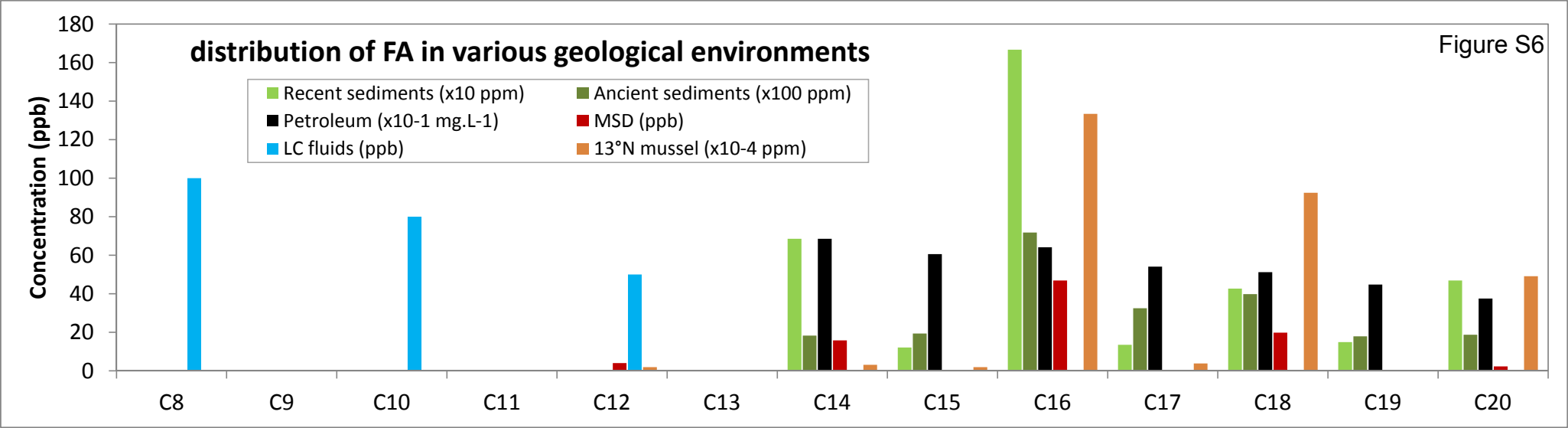
distribution of FA in various geological environments
Figure S6
Recent sediments (x10 ppm)
Ancient sediments (x100 ppm)
Petroleum (x10-1 mg.L-1)
MSD (ppb)
LC fluids (ppb)
13°N mussel (x10-4 ppm)
Concentration (ppb)
180
160
140
120
100
80
60
40
20
0
C8
C9
C10
C11
C12
C13
C14
C15
C16
C17
C18
C19
C20

Figure S7

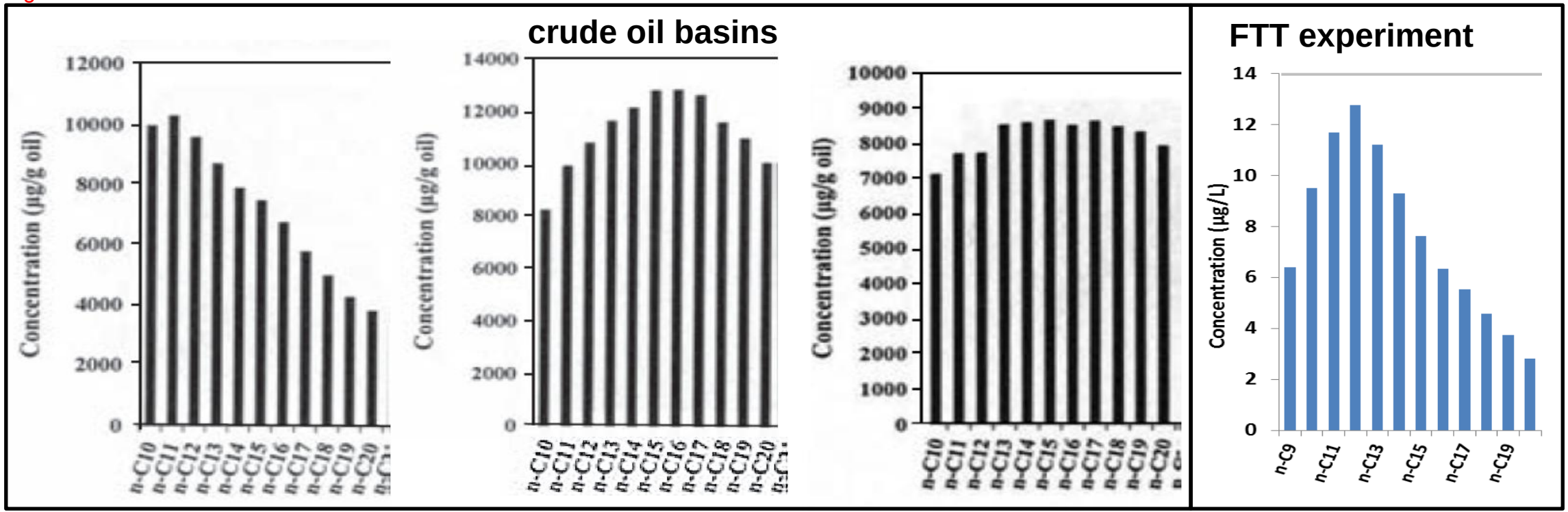
crude oil basins
FTT experiment
Concentration (μg/g oil)
Concentration (μg/L)
n-C10
n-C11
n-C12
n-C13
n-C14
n-C15
n-C16
n-C17
n-C18
n-C19
n-C20
n-C9

Figure S11

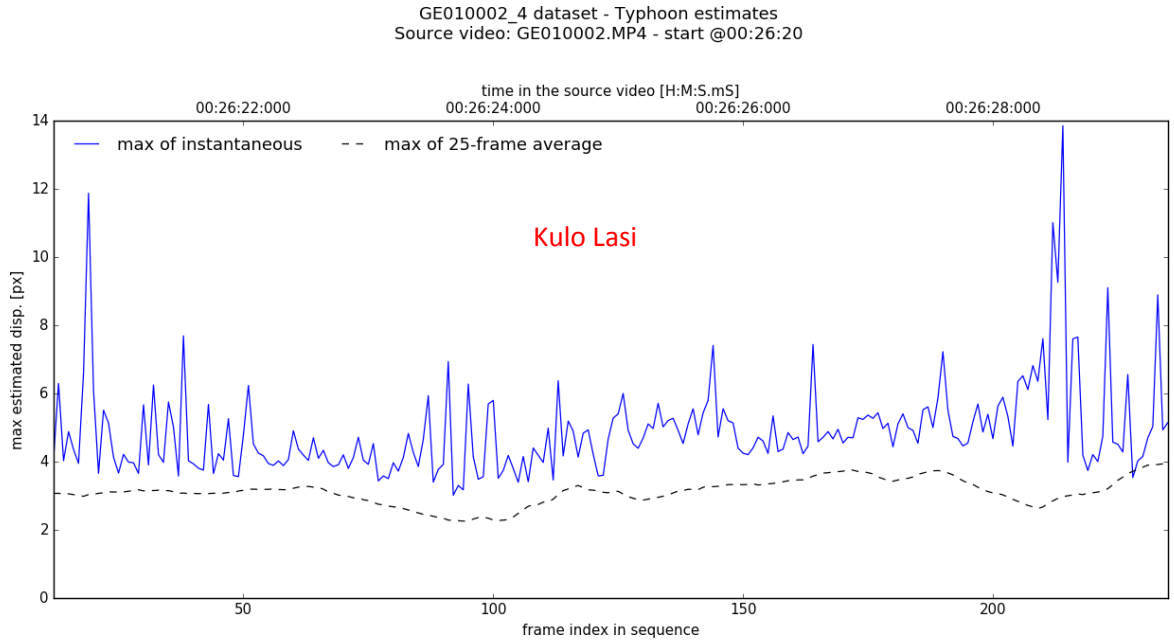
GE010002_4 dataset - Typhoon estimates
Source video: GE010002.MP4 - start @00:26:20
time in the source video [H:M:S.mS]
00:26:22:000
00:26:24:000
00:26:26:000
00:26:28:000
max of instantaneous
max of 25-frame average
Kulo Lasi
max estimated disp. [px]
frame index in sequence

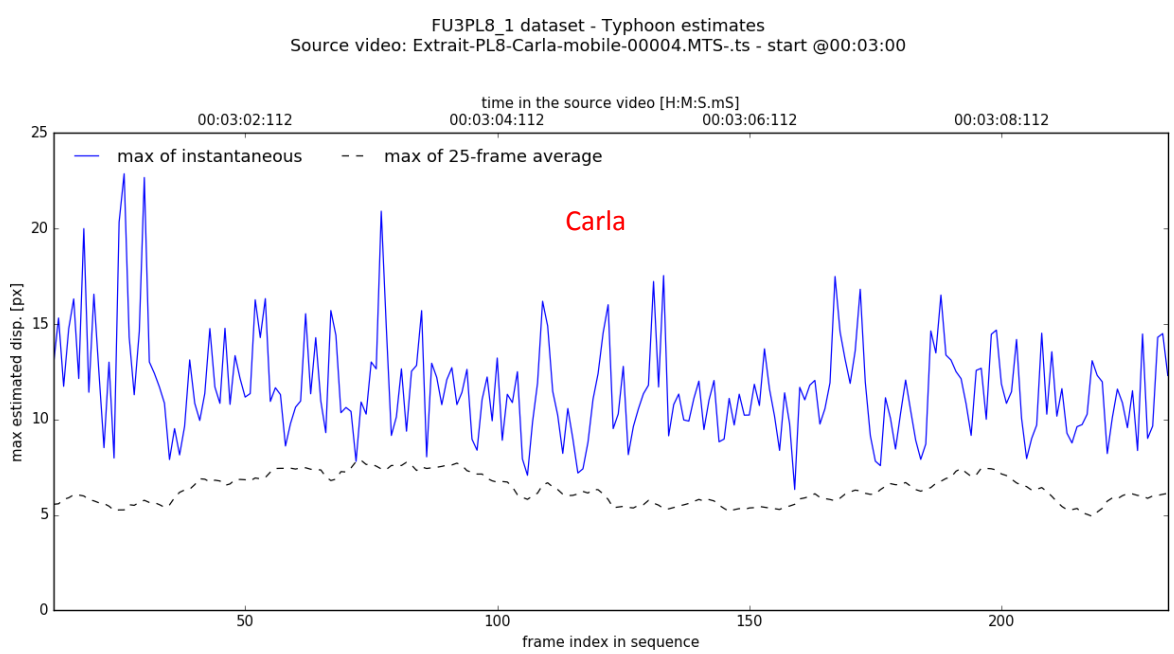
FU3PL8_1 dataset - Typhoon estimates
Source video: Extrait-PL8-Carla-mobile-00004.MTS-.ts - start @00:03:00
time in the source video [H:M:S.mS]
00:03:02:112
00:03:04:112
00:03:06:112
00:03:08:112
max of instantaneous
max of 25-frame average
Carla
max estimated disp. [px]
frame index in sequence

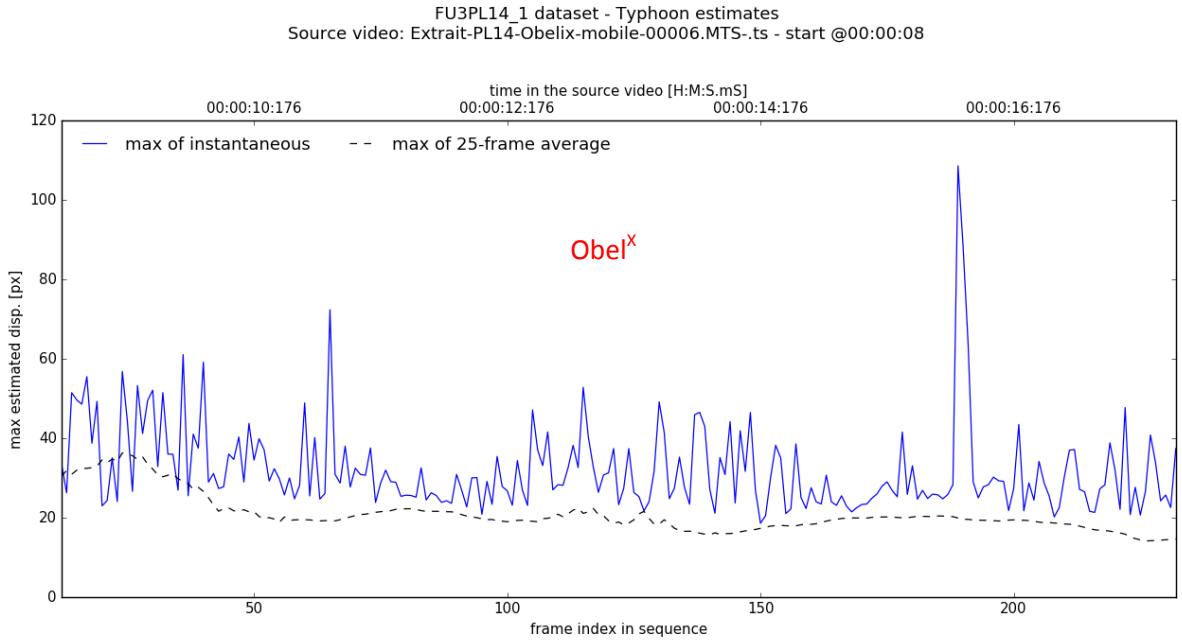
FU3PL14_1 dataset - Typhoon estimates
Source video: Extrait-PL14-Obelix-mobile-00006.MTS-.ts - start @00:00:08
time in the source video [H:M:S.mS]
00:00:10:176
00:00:12:176
00:00:14:176
00:00:16:176
max of instantaneous
max of 25-frame average
Obel^X
max estimated disp. [px]
frame index in sequence